Atomic-layer-resolved composition and electronic structure of the cuprate $Bi_2Sr_2CaCu_2O_{8+\delta}$ from soft x-ray standing-wave photoemission

Cheng-Tai Kuo[1,2*], Shih Chieh Lin[1,2], Giuseppina Conti[1,2], Shu-Ting Pi[1], Luca Moreschini[3], Aaron Bostwick[3], Julia Meyer-Ilse[2], Eric Gullikson[2], Jeffrey B. Kortright[2], Slavomir Nemšák[4], Julien E. Rault[5], Patrick Le Fèvre[5], François Bertran[5], Andrés F. Santander-Syro[6], Ivan A.Vartanyants[7,8], Warren E. Pickett[1], Romuald Saint-Martin[9], Amina Taleb-Ibrahimi[5], Charles S. Fadley[1,2]

[1]*Department of Physics, University of California Davis, Davis, California 95616, USA*
[2]*Materials Sciences Division, Lawrence Berkeley National Laboratory, Berkeley, California 94720, USA*
[3]*Advanced Light Source, Lawrence Berkeley National Laboratory, Berkeley, California 94720, USA*
[4]*Peter Grünberg Institut PGI-6, Research Center Jülich, 52425 Jülich, Germany*
[5]*Synchrotron SOLEIL, L'Orme des Merisiers, Saint-Aubin-BP48, 91192 Gif-sur-Yvette, France*
[6]*CSNSM, Université Paris-Sud, CNRS/IN2P3, Université Paris-Saclay, 91405 Orsay Cedex, France*
[7]*Deutsches Elektronen-Synchrotron DESY, Notkestraße 85, D-22607 Hamburg, Germany*
[8]*National Research Nuclear University MEPhI (Moscow Engineering Physics Institute), Kashirskoe Shosse 31, Moscow, 115409, Russia*
[9]*SP2M-ICMMO-UMR-CNRS 8182, Université Paris-Sud, Université Paris-Saclay, 91405 Orsay Cedex, France*
*chengtaikuo@lbl.gov

An important challenge remaining in the high-temperature superconductor cuprates is the unambiguous differentiation of the composition and electronic structure of the CuO_2 layers and those of the intermediate layers. The large c lattice constant for these materials permits employing soft x-ray (930.3 eV) standing wave (SW) excitation in photoemission with layer-by-layer depth resolution of these properties. We present a soft x-ray SW photoemission study of $Bi_2Sr_2CaCu_2O_{8+\delta}$ (Bi2212), deriving the depth distribution of atomic composition within its unit cell and successfully deconvoluting the electronic structure into the atomic-layer-resolved cross-section-weighted densities of states (DOSs). Significant Ca-Sr intermixing is quantitatively determined and the oxygen states bonding to different cations are resolved. The layer-resolved DOSs of Bi2212 show good agreement with DFT calculations, provided that we incorporate the supermodulation structures. Future measurements of this type for other quasi-two-dimensional materials with large-c should yield unique information on their atomic-layer-resolved composition and electronic structure.

The cuprate high-temperature superconductors have attracted much attention and been extensively studied, but are still not fully understood. It is believed that superconductivity is related to hole- or electron- doping within their layered quasi-2D crystallographic structures, with the key element being the CuO_2 planes[1,2]. Characterizing this basic element in superconductivity is thus critical, and some important challenges remaining are to differentiate the electronic structure of the CuO_2 layers from those of the intermediate layers, as well as the elemental composition of each layer.

Photoemission spectroscopy, especially angle-resolved photoemission spectroscopy (ARPES), is one of the most powerful techniques for visualizing the electronic structure in materials[1,3,4]. Conventional ARPES measurements are performed with excitation energies of ~20 to 150 eV that yield high surface sensitivity due to the short electron inelastic mean-free paths[5] of ~3-6 Å. For materials with small unit-cell dimensions perpendicular to the surface and inert, easily cleavable or *in situ*-preparable surfaces, ARPES can provide unique information on properties close to that of bulk. However, for materials with large c-axis parameters, e.g. the cuprates, it can be argued that conventional ARPES preferentially samples the topmost atomic layers rather than the full unit cell. For example, in the case of $Bi_2Sr_2CaCu_2O_{8+\delta}$ (Bi2212), the c-axis parameter is ~30.7 Å, and its first CuO_2 layer in the unit cell is ~6 Å below the cleaved surface; thus, for conventional ARPES, the contributions from the first CuO_2 layer will be attenuated by ~ $e^{-1} = 0.37$, and they will be even more extreme for the deeper layers. Beyond this, in conventional ARPES, the only way to distinguish element-specific behavior is to use resonant photoemission (RPE) that would selectively enhance the different layer

contributions[6,7]. But quantitative interpretation of RPE is difficult, and the number of elements that can be studied is limited by the suitable core levels to excite resonantly. Standing-wave (SW) photoemission provides a method to get around these limitations of conventional ARPES and RPE.

X-ray SW excitation with energy ~2-10 keV in connection with spectroscopy was introduced some time ago[8], and its theory and applications have been reviewed in detail recently[9]. SW *hard x-ray* photoemission at a few keV has been used to derive the spatial distribution of composition and differentiate the element-specific matrix-element weighted densities of states (DOSs) within the unit cells of several solids[10,11,12], including $YBa_2Cu_3O_{7-\delta}$[13]. For higher photon energies above the ca. 1 keV regime, these DOSs can be considered to be weighted by differential atomic-cross sections, and it is at this level that we will analyze our data.

In this work, we have used *soft x-ray* photoemission at 930.3 eV to study Bi2212, utilizing its (002) Bragg reflection to generate the SW, with the lower energy enabling higher energy resolution and greater sensitivity to electron momentum than the hard x-ray studies. A photon energy of 930.3 eV was further chosen near an absorption resonance to maximize the SW strength; see the detail in Supplementary Information S2.

A SW with its iso-intensity planes parallel to the diffracting planes is created by the interference between the incident ($\boldsymbol{k}_0$) and diffracted ($\boldsymbol{k}_{002}$) waves[9], as illustrated in Fig. 1. Figure 1a shows the Bi2212 crystallographic structure of the top half unit cell, and its

cleavage plane primarily occurs in between the BiO layers due to weak van der Waals bonds[1]. The Bi, Sr, Cu, and Ca cations in these layers are well separated along the c-axis direction, making Bi2212 an ideal candidate for applying the SW technique to derive layer-resolved information. From SW theory based on dynamical x-ray diffraction[8,9], the phase difference between the incident and diffracted wave fields changes by π when the incidence angle moves from below to above the Bragg condition, thus scanning the SW by $d_{002}/2$ with respect to the (002) planes, as illustrated in Figs. 1b,c. The detailed theoretical SW modeling, including consideration of both x-ray and electron attenuation with depth, is discussed in Supplementary Information S3. Depending on the locations of the atoms with respect to the scanned SW, the incidence-angle dependence of the core-level photoelectron intensities, which we define as core-level rocking curves (RCs), will show distinct modulations as to both shape and magnitude.

Figures 2 and 3 illustrate the layer-dependent results for core-level intensities using SW excitation. The photoelectron spectra of Ca 2p, Sr 3d, Cu 3p, and Bi $4f_{7/2}$ at an off-Bragg angle (23.2°) are shown in Figs. 2a-d. Such photoelectron spectra were collected by varying the incidence angle between 24° and 27.5°, yielding the five distinct core-level RCs in Figs. 2e-i. These RCs are normalized to 1 at off-Bragg positions and have been simulated by SW theory (red curves in Figs. 2e-i). Both members of the spin-orbit split Ca 2p spectrum (Fig. 2a) exhibit two components, with low-binding-energy (LBE) peaks at 344.6 and 348.1 eV and high-binding-energy (HBE) features at 345.9 and 349.4 eV. These have been observed in previous XPS studies, with varying relative intensities, depending on the sample synthesis procedure[6,14,15,16]. The RCs of the Ca 2p(LBE) in Fig.

2e and Ca 2p(HBE) in Fig. 2f show different shapes and relative intensity modulations, with LBE exhibiting higher modulation ~8%, as compared to ~5% for HBE. The experimental Ca 2p(HBE) RC is, within statistical noise, also identical to the Sr 3d RC (Fig. 2g), including the amplitude of modulation, suggesting that the depths of Ca(HBE) and Sr atoms are essentially identical. Thus, we can unambiguously conclude that the Ca(LBE) atoms are located in the Ca layer, while the Ca(HBE) atoms are located in the SrO layer, implying that a significant fraction of Ca atoms occupy the Sr sites during synthesis.

A more quantitative analysis was made by considering the peak intensity ratio, I(HBE)/[I(HBE)+I(LBE)] away from the Bragg reflection, which is ~0.2; this indicates that an excess of ~10% Ca intermixing with each of the two adjacent SrO layers. Previous work on the degree of Sr-Ca intermixing is controversial[6,14,15,16], with some studies suggesting pronounced Sr-Ca intermixing in both Ca and SrO layers[14] and some claiming low intermixing but with strong dependence on sample preparation[15,16]. For our sample, both the observation of only one component in the Sr 3d spectrum and its RC show that the Sr atoms are located in a single layer without intermixing. The Cu 3p and Bi 4f spectra in Figs. 2c,d also show single components, although Cu 3p is broad, as seen previously[7], and their very different RCs (Figs. 2h,i) demonstrate that the Cu and Bi atoms are uniquely located in their own layers. Note that the *shape* of the Sr 3d and Cu 3p RCs are close, which is not surprising in view of the location of Sr atoms on either side of the Cu atoms, but the Cu 3p RC shows a stronger intensity modulation due to the lack of SW phase averaging over the two Sr layers in the half unit cell. All of these

conclusions are supported by the excellent agreement between experiment and SW modeling in Figs. 2e-i.

We now consider the O 1s spectrum in Fig. 3a, which is thought from prior XPS work to exhibit three components contributed from the different atomic layers[17,18]. Through modeling the O1s RCs with SW theory, the locations of these components were determined. The O 1s(P1) RC (Fig. 3b) shows that these oxygen atoms are located in the BiO layer. The O 1s(P2) RC in Fig. 3c has a similar shape but weaker intensity modulation compared to the Cu 3p RC, suggesting that, in the first CuO layer, the O(P2) atoms is ~0.9±0.5 Å higher than Cu atoms. O 1s(P3) RC (Fig. 3d) is slightly out of phase with respect to the Sr 3d RC, suggesting that, in the first SrO layer, the P3 oxygen atoms are ~1.5±0.5 Å higher relative to Sr atoms. These SW-determined locations of the oxygen atoms are in good agreement with prior transmission electron microscopy and x-ray diffraction results[19,20]. Looking ahead, future SW photoemission studies of Bi2212 or other cuprates, with higher reflectivities and better statistics, and with various oxygen dopant levels, should be able to determine the O stoichiometries in each layer and thus answer the question of where the additional oxygen dopant atoms reside.

In order to resolve the individual atomic layer contributions to the Bi2212 valence band (VB), we measured the VB RCs, which is an intensity map $I_{VB}(E_b, \theta_{inc})$, with binding energy ($E_b$) and incidence angle ($\theta_{inc}$), over an angle scan. The VB RCs can be written as a superposition of the experimentally layer-projected and cross-section weighted DOSs in the different layers, $D_i(E_b) \approx \sum_{i,Qnl} \frac{d\sigma_{Qnl}}{d\Omega} \rho_{Qnl}(E_b)$, multiplied by layer-dependent normalized

core-level RCs $\overline{I}_{Qn'\ell'}(\theta_{inc})$, as discussed previously[11,12,13,21,22,23,24], see further details in Supplementary Information S4. That is,

$$I_{VB}(E_b,\theta_{inc}) = \sum_{Qn\ell} D_{Qn\ell}(E_b)\overline{I}_{Qn'\ell'}(\theta_{inc}) \ . \qquad (1)$$

Here $Qn\ell$ denotes a valence level $n\ell$ in the atom Q, and $Qn'\ell'$ a core level in the same atom, and $\overline{I}_{Qn'\ell'}(\theta_{inc})$ is the RC for $Qn'\ell'$, normalized to unity away from the Bragg reflection. For our case, $Qn'\ell'$ = Cu 3p, Sr 3d, and Bi $4f_{7/2}$.

The main contributions from the atomic orbitals in the layer-projected DOSs based on strength of hybridization and photoelectric cross sections at our excitation energy are Cu 3d in CuO_2, Sr 4p in SrO, and Bi 5d in BiO (see Supplementary Information S5). The Ca 4s orbitals in the Ca layer are negligible, as discussed in prior work using density functional theory (DFT) calculations in the local-density approximation (LDA)[25,26]. In both the raw data for $I_{VB}(E_b, \theta_{inc})$ of Fig. 4a and in a more pronounced way in its second derivative along the axis of incidence angle in Fig. 4b, there are intensity modulations with BE associated with the different layer contributions to the intensity; these are particularly clear along the Bragg angle at ~25.7°. The VB RCs for each BE have been fitted to a linear combination of these three core-level RCs by a least-squares method, and the resultant fitting coefficients correspond to the layer-resolved cross-section weighted DOSs $D_i(E_b)$.

Fig. 4c shows these experimental layer-projected cross-section-weighted DOSs (dots) in comparison to DFT calculations (curves) incorporating the supermodulation (SM)

displacements known to exist in Bi2212[19], in particular with a twofold enlargement of the unit cell size in the x-y plane (see Supplementary Information S6). The $D_{CuO_2}(E_b)$ and $D_{BiO}(E_b)$ show good agreement with the DFT results including SM. The $D_{SrO}(E_b)$ is however considerably broader than the DFT results. One obvious source of uncertainty and broadening has been mentioned before: the Sr 3d RC has similar shape compared to the Cu 3p RC, meaning that the deconvolution procedure will inherently mix some intensity from CuO_2. Beyond this, the broadening of $D_{SrO}(E_b)$ is certainly associated with the significant Ca-Sr intermixing, causing more disorder and scattering. Further electronic structure calculations, e.g. within the coherent potential approximation (CPA), would help to test this hypothesis.

To assist in understanding the influence of the SM atomic displacements on the electronic structure, the layer-projected DOSs with and without SM are plotted together in Fig. 4d. The introduction of SM makes no significant difference in the CuO_2 DOS, but for both cases, a shift to higher BE by 1.3 eV is necessary to reach agreement with the experimental $D_{CuO_2}(E_b)$. For the SrO and BiO DOSs, no BE shift is needed for the SM results, whereas without SM, one needs to shift the curves to higher BE by 0.9 eV and to lower BE by 1.3 eV to best match experiment, respectively. Adding SM for the SrO DOS further produces an additional peak at ~5 eV that much better matches the experimental $D_{SrO}(E_b)$. For the BiO plane, the disappearance of a peak at ~6.5 eV in the theoretical DOS with SM structure is again in better agreement with the experimental $D_{BiO}(E_b)$. In summary, taking SM into consideration leads to a change of the SrO and BiO DOSs,

improving the agreement with the layer-projected DOSs. This indicates the strong influence of the SM structure on the electronic structure of Bi2212.

We have noted that an energy shift of the theoretical CuO_2 DOS to 1.3 eV higher BE has been necessary to match the $D_{CuO_2}(E_b)$. Such shifts of the VB energies in photoemission relative to LDA calculations have been widely reported in the cuprates (e.g. LSCO[27], YBCO[27], and Bi2212[28]). The Coulomb interaction between the Cu 3*d* electrons in cuprates, which is not treated fully in simple DFT calculations, can lead to the opening of a Mott-Hubbard gap, with a bound-state energy shift to higher BE and a lower DOS in the vicinity of the Fermi energy (E_F)[27,28]. These features in the cuprate VBs are spectroscopic evidence of strong correlation effects, and more detailed discussions can be found elsewhere[29]. The $D_{CuO_2}(E_b)$ thus shows an energy shift that can be attributed to this electron correlation effect.

In order to visualize in more detail the layered-resolved electronic structure of Bi2212, the band structures near the E_F region are shown in Fig. 5. The full band structure without SM is shown in Fig. 5a, and in Fig. 5b with SM. The band structure in Fig. 5a is in good agreement with prior work[25,26]. By comparing these two figures, one clearly sees a splitting of the bands (at ~-2 eV and at 0.5 to 2 eV BE) that results from including SM. For the more realistic band structure with SM we now show the layer-projected band structures in Figs. 5c-e in a blue-gray scale to indicate relative amplitude. From these results alone, one would conclude that, around the M point, the Fermi surface of Bi2212 is governed by the CuO_2 bands, but that there is also a strong contribution from BiO

bands. Although our DFT results show the existence of BiO bands near the M point (Fig. 5e) and some BiO state intensity extending below E_F (Fig. 4c), our experimental results in the same figure lack that spectral feature, in agreement with previous photoemission studies[1,6]. For example, to resolve this disagreement between the DFT results and photoemission, Lin *et al.*[30] proposed that, with increasing oxygen doping in the BiO layer, the BiO band shifts above E_F at the M point, which also is consistent with a scanning tunneling microscopic and spectroscopic study[31]. The excess oxygen atoms are believed to be responsible for the δ in the common designation $Bi_2Sr_2CaCu_2O_{8+\delta}$.

In summary, we have carried out soft x-ray SW photoemission study of Bi2212 and derived the depth distribution of atoms within one unit cell, in particular, a 10% Ca-Sr intermixing and the three types of oxygen atoms bonding to different cations. In addition, we have successfully decomposed the electronic structure of Bi2212 into atomic-layer-specific, matrix-element-weighted DOSs. These atomic-layer-resolved DOSs show good agreement with DFT calculations in most respects, provided we incorporate the known supermodulation structure in Bi2212. Our results for the layer-resolved electronic structure are found to be strongly influenced by the SM structure, Ca-Sr intermixing, and the Cu 3d-3d Coulomb interaction, further clarifying the complexity of this prototypical cuprate. Future measurements of this type for other cuprates or other materials such as topological insulators with large c axes should yield equally unique information. Bragg-reflection SW photoemission is thus very promising for the study of quasi-two-dimensional materials with large-c lattice parameters.

Methods

Experimental methods. For our $Bi_2Sr_2CaCu_2O_{8+\delta}$ (Bi2212) single crystal, the critical temperature determined by SQUID is ~93K. X-ray reflectivity measurements were performed at beamline 6.3.2 of Advanced Light Source (ALS). The Cr absorption edge (574.1 eV) is used for the energy calibration. Angle-resolved photoemission spectroscopy, x-ray absorption spectroscopy (XAS) and standing-wave excited photoemission (SW-XPS) measurements were performed at beamline 7.0.2 (MAESTRO) of ALS, and the beamline CASSIOPEE of SOLEIL. Details concerning the sample growth and characterization are in Supplementary Information S1.

Theoretical calculations. The reflectivity and SW RC data were analyzed using SW theory based on dynamical x-ray diffraction. The resonant Cu atomic scattering factors were calculated from a Cu L_3 XAS spectrum using Kramers-Kronig relations. The atomic coordinates of Bi2212 with SM structure were obtained from Ref. 19. The electronic structures were calculated using the first-principles package Quantum Espresso[32] with generalized gradient approximation (GGA)[33] for the correlation functional, optimized norm-conserving Vanderbilt pseudopotenetials [34] with spin-orbit coupling for core electrons, 10×10×2 for k-sampling integration and 40 Ry for energy cutoff. Further details are in Supplementary Information.

Acknowledgements

The authors would like to thank Jonathan Denlinger and Simon Moser for their comments concerning Bi2212 sample preparation. We thank synchrotron SOLEIL (via Proposal No. 20161205) for access to Beamline CASSIOPEE that contributed to the results presented here. This work was supported by the US Department of Energy under Contract No. DE-AC02-05CH11231 (Advanced Light Source), and by DOE Contract No. DE-SC0014697 through the University of California Davis (salary for C.-T.K, S.C.L. and C.S.F.). S.-T. Pi was supported by DOE grant DE-NA0002908. C.S.F. has also been supported for salary by the Director, Office of Science, Office of Basic Energy Sciences (BSE), Materials Sciences and Engineering (MSE) Division, of the U.S. Department of Energy under Contract No. DE-AC02-05CH11231, through the Laboratory Directed Research and Development Program of Lawrence Berkeley National Laboratory, through a DOE BES MSE grant at the University of California Davis from the X-Ray Scattering Program under Contract DE-SC0014697, through the APTCOM Project, "Laboratoire d'Excellence Physics Atom Light Matter" (LabEx PALM) overseen by the French National Research Agency (ANR) as part of the "Investissements d'Avenir" program, and from the Júlich Research Center, Peter Grűnberg Institute, PGI-6. Support for W.E.P. was provided by DOE grant DE-FG02-04ER46111. This research used resources of the National Energy Research Scientific Computing Center (NERSC), a DOE Office of Science User Facility supported by the Office of Science of the U.S. Department of Energy under Contract No. DE-AC02-05CH11231.

Author contributions

C.-T.K and S.C.L. carried out the ARPES and SW-XPS measurements using the MAESTRO beamline with assistance from L.M., A.B., and C.S.F., and using the beamline CASSIOPEE with assistance from J.E.R., P.L.F., F.B., and A.T.; J.M.-L. and

C.-T.K. performed soft x-ray reflectivity measurements with assistance from E.G.; C.-T.K. carried out dynamical diffraction calculations with feedback and discussions from I.V., J.B.K., and C.S.F.; S.-T.P. and W.E.P. carried out DFT calculations. A.F.S.-S. and C.S.F. conceived the project. R.S.-M. supplied the Bi2212 crystals. C.-T.K. carried out the data analysis and wrote the manuscript under the supervision of I.V. and C.S.F. All authors contributed to the manuscript.

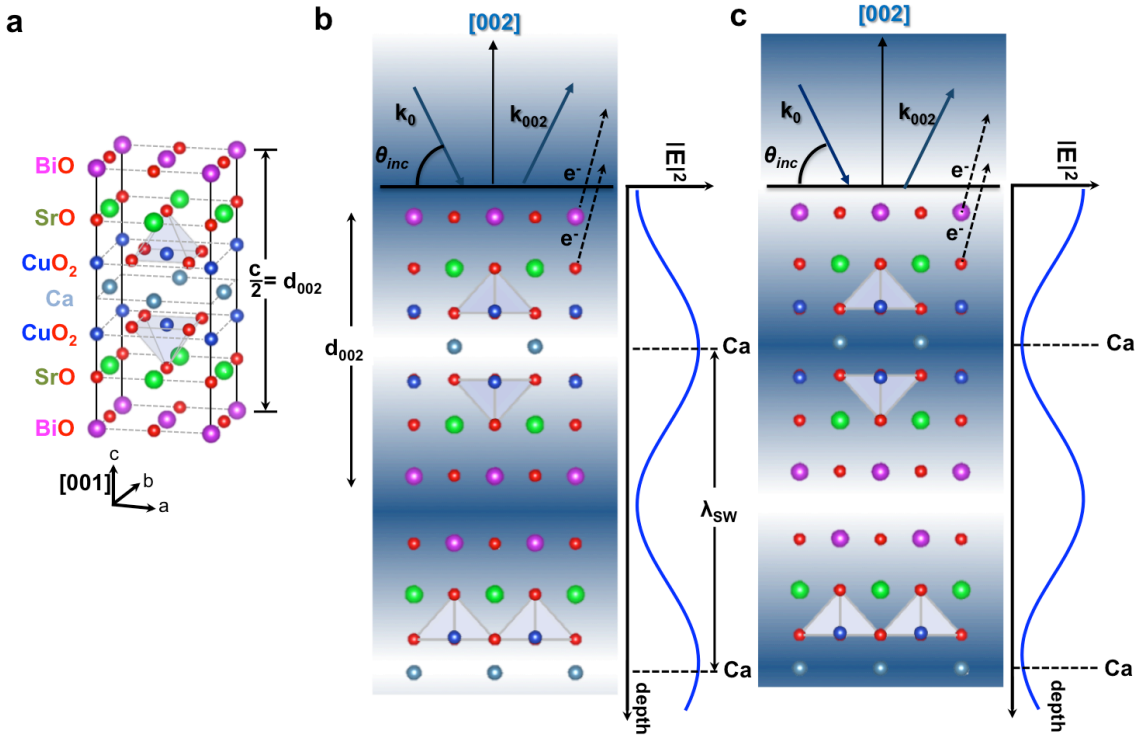

Figure 1 Spatial relationship between the $Bi_2Sr_2CaCu_2O_{8+\delta}$ (Bi2212) crystal planes and the (002) Bragg-reflection x-ray standing wave (SW). a, Top half of the unit cell of Bi2212. **b,** Schematic of the experimental geometry and the SW generated by the Bi2212 (002) reflection, with wavelength = $\lambda_{SW} = c/2 = d_{002}$. The incident and diffracted waves (associated with wave vectors $\boldsymbol{k_0}$ and $\boldsymbol{k_{002}}$) interfere to produce the SW. The photon energy was 930.3 eV, with a corresponding Bragg angle of about 25.7°. **c,** By increasing the incidence angle around the (002) Bragg reflection, the SW can be shifted by $d_{002}/2$. The maximum of the SW electric field intensity can thus be shifted continuously from the Ca plane (**b**) to the BiO plane (**c**).

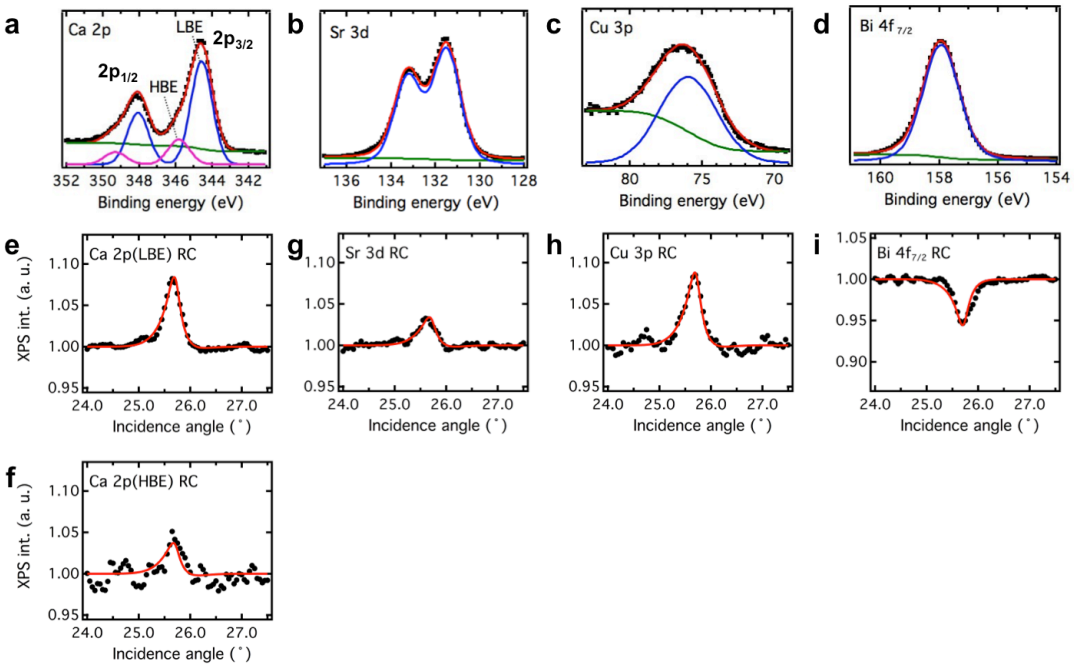

Figure 2 Bragg-reflection standing-wave x-ray photoemission from the cations of Bi2212 at *hv* = 930.3 eV. Core-level spectra of **a**, Ca 2p, **b**, Sr 3d, **c**, Cu 3p, and **d**, Bi $4f_{7/2}$ at an off-Bragg incidence angle. The core-level peak intensities are derived by fitting with a Voigt line shape (in blue and magenta) and a Shirley background (in green). The corresponding experimental rocking curves (RCs) of core-level intensities are also plotted in **e-i** (black dots) and compared with SW theory (red curves). In **a**, Ca 2p is found to have high-binding-energy (HBE) and low-binding-energy (LBE) components, which shows different RC behavior as to shape and fractional modulation. The RCs of Ca 2p HBE (in **f**) and Sr 3d (in **g**) are found to be identical within experimental error, indicating that Ca atoms occupy the Sr sites in the SrO layer.

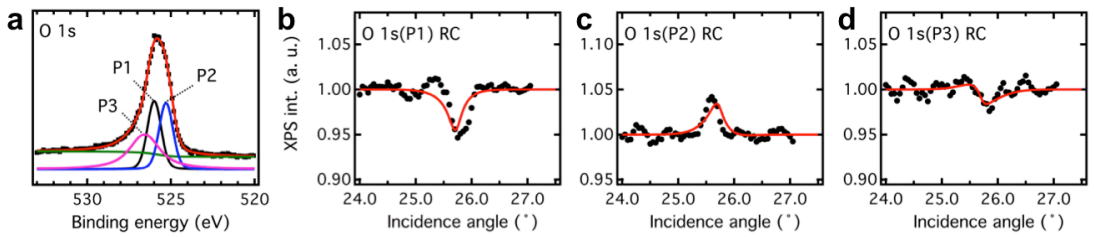

Figure 3 Bragg-reflection standing-wave x-ray photoemission from the oxygen atoms of Bi2212. a, Core-level spectrum of O 1s at an off-Bragg incidence angle. The O1s spectrum is known to contain three components (P1, P2, and P3). The RCs of **b**, P1, **c** P2, and **d**, P3 exhibit distinct shape and intensity modulations; these can be assigned through SW analysis (red curves) to different layers. The O(P1) atoms are located in the BiO layer. The O(P2) atoms are in the CuO_2 layer with a vertical offset of ~0.9±0.5 Å to the Cu atoms. The O(P3) atoms are in the SrO layer with a vertical offset of ~1.5±0.5 Å.

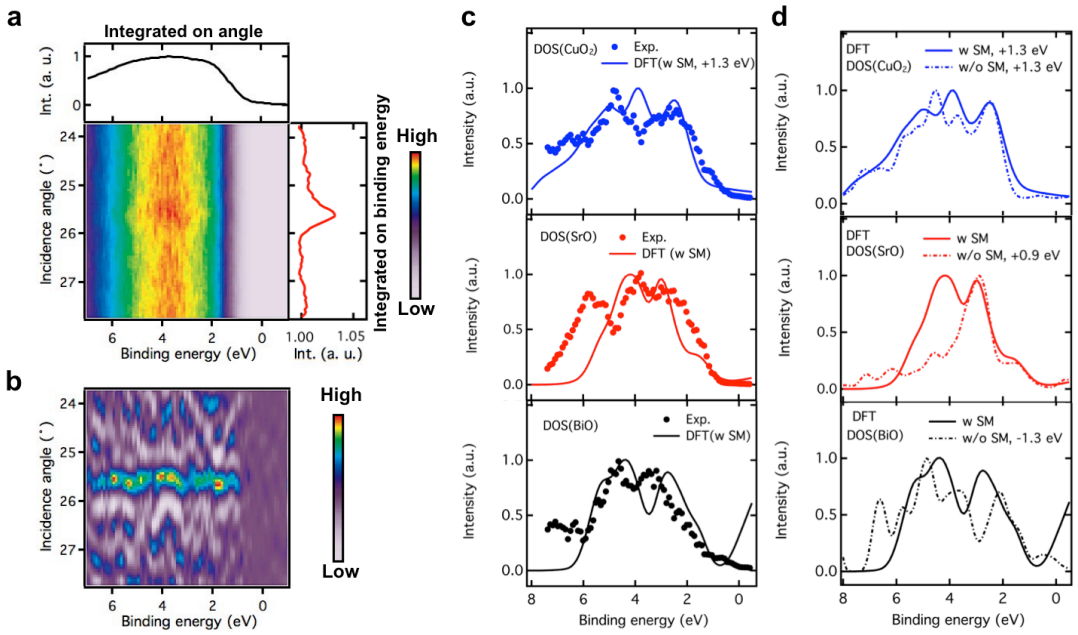

Figure 4 Standing-wave valence-band (VB) spectra and atomic-layer-resolved, cross-section-weighted densities of states (DOSs) together with DFT calculations. a, VB intensity map for different incidence angles, with the color scale corresponding to the photoemission intensity, and top and right curves representing integrals over incidence angle and binding energy, respectively. **b,** As **a** , but for the second-derivative of intensity. The Bragg–reflection maximum is at ~25.7°, and the VB intensities exhibit modulations that are associated with the variable layer-specific contributions along the binding energy axis; this is particularly evident in the second derivative plot. **c,** The layer-projected DOSs of CuO_2 (blue dots), SrO (red dots), and BiO (black dots) and the corresponding layer-projected DOSs from DFT calculations including supermodulation in the crystal structure (solid line). **d**, The comparison of DFT results with supermodulation (w SM) structures (solid line) and without supermodulation (w/o SM) structures are shown (dot-dashed line). Various energy shifts have been applied to theory in **c** and **d** to yield the best agreement with experiment; with SM, only the CuO_2 DOS requires a shift.

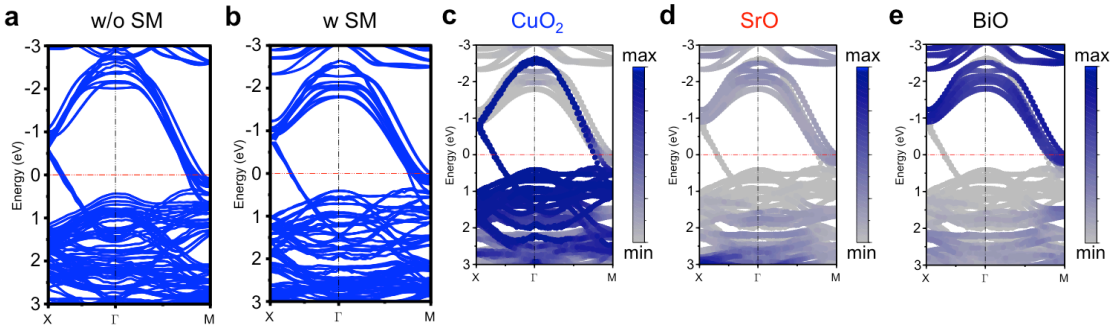

Figure 5 Band structure in the high-symmetry directions near the E_F. a,b, Full band structure for Bi2212 without (**a**) and with (**b**) supermodulation effect in the crystal structure. **c,d,e** The layer-projected (CuO_2, SrO, and BiO) band structures of **b** (with SM). The blue-to-grey color scale indicates strong-to-weak contribution from a given layer.

[1] Damascelli, A., *et al.* Angle-resolved photoemission studies of the cuprate superconductors. *Rev. Mod. Phys.* **75**, 473-541 (2003).
[2] Fisher, Ø. *et al.* Scanning tunneling spectroscopy of high-temperature superconductors. *Rev. Mod. Phys.* **79**, 353-419 (2007).
[3] Himpsel, F. J. Angle-resolved measurements of the photoemission of electrons in the study of solides. *Adv. Phys.* **32**, 1-51 (1983).
[4] Hasan, M. Z. and Kane, C. L. Topological insulators. *Rev. Mod. Phys.* **82**, 3045-3067 (2010).
[5] Tanuma, S. *et al.* Calculation of electron inelastic mean free paths. IX. Data for 41 elemental solids over the 50 eV to 30 keV range. *Surf. Interface Anal.* **43**, 689-713 (2011).
[6] Lindberg, P. A. P. *et al.* Photoemission studies of high-temperature superconductors. *Surf. Sci. Rep.* **11**, 1-137 (1990).
[7] Qvarford, M. *et al.* Resonant valence-band and Cu 3*p* photoemission at the Cu L_3 threshold of $Bi_2Sr_2CuO_6$ and $Bi_2Sr_2CaCu_2O_8$. *Phys. Rev. B* **51**, 410-416 (1995).
[8] Batterman, B. W. and Cole, H. Dynamical diffraction of x rays by perfect crystals. *Rev. Mod. Phys.* **36**, 681-717 (1964).
[9] Vartanyants, I. A. and Kovalchuk, M. V. Theory and applications of x-ray standing waves in real crystals. *Rep. Prog. Phys.* **64**, 1009-1084 (2001).
[10] Woicik, J. C. *et al.* Direct measurement of valence-charge asymmetry by x-ray standing waves. *Phys. Rev. Lett.* **84**, 773-776 (2000).
[11] Woicik, J. C. *et al.* Partial density of occupied valence states by x-ray standing waves and high-resolution photoelectron spectroscopy. *Phys. Rev. B* **63**, 041403R (2001).
[12] Thiess, S. *et al.* Valence band photoelectron emission of $STiO_3$ analyzed with X-ray standing waves. *Sol. Stat. Comm.* **150**, 553-556 (2010).
[13] Thiess, S. *et al.* Resolving CuO chain and CuO_2 plane contributions to the $YBa_2Cu_3O_{7-\delta}$ valence band by standing-wave excited hard x-ray photoelectron spectroscopy. *Phys. Rev. B* **92**, 075117 (2015).
[14] Kohiki, S. *et al.* Photoemission from single-crystalline Bi-Sr-Ca-Cu-O. *Phys. Rev. B* **38**, 7051-7053 (1988).
[15] Hillebrecht, F. U. *et al.* Experimental electronic structure of $Bi_2CaSr_2Cu_2O_{8+\delta}$. *Phys. Rev. B* **39**, 236-242 (1989).
[16] Meyer, H. M. III, *et al.* Occupied electronic states of single-crystal $Bi_2Ca_{1+x}Sr_{2-x}Cu_2O_{8+y}$. *Phys. Rev. B* **38**, 7144-7147 (1988).
[17] Parmigiani, F. *et al.* O 1*s* core levels in $Bi_2Sr_2CaCu_2O_{8+\delta}$ single crystals. *Phys. Rev. B* **43**, 3085-3090 (1991).
[18] Qvarford, M. *et al.* Doping dependence of the O 1*s* core-level photoemission in Bi-Sr-Ca-Cu-O superconductors. *Phys. Rev. B* **53**, R14753-R14756 (1996).
[19]Hervieu, M. *et al.* Electron microscopy study of the superconductor "$Bi_2Sr_2CaCu_2O_{8+\delta}$". *Mod. Phys. Lett. B* **2**, 491-500 (1988).
[20] Sunshine, S. A. *et al.* Structure and physical properties of single crystals of the 84-k superconductor $Bi_{2.2}Sr_2Ca_{0.8}Cu_2O_{8+\delta}$. *Phys. Rev. B* **38**, 893-896 (1988).
[21] Kaiser, A. M. *et al.* Suppression of near-Fermi level electronic states at the interface in a $LaNiO_3/SrTiO_3$ superlattice. *Phys. Rev. Lett.* **107**, 116402 (2011).
[22] Gelius, U. in *Electron Spectroscopy*, Shirley, D. A. Ed. (North Holland, 1971) p. 311

[23] Solterbeck, C. *et al.* Energetic and spatial bonding properties from angular distributiona of ultraviolet photoelectrons: Applications to the GaAa(110) surface. *Phys. Rev. Lett.* **79**, 4681-4684 (1997).
[24] Gray, A. X. *et al.* Bulk electronic structure of the dilute magnetic semiconductor $Ga_{1-x}Mn_xAs$ through hard x-ray angle-resolved photoemission. *Nat. Mater.* **11**, 957-962 (2012).
[25] Krakauer, H. and Pickett, W. E. Effect of Bismuth on high-Tc cuprate superconductors: Electronic structure of $Bi_2Sr_2CaCu_2O_8$. *Phys. Rev. Lett.* **60**, 1665-1667 (1988).
[26] Mattheiss, L. F. and Hamann D. R. Electronic band properties of $CaSr_2Bi_2Cu_2O_8$. *Phys. Rev. B* **38**, 5012-5015 (1988).
[27] Fujimori, A. *et al.* Spectroscopic evidence for strongly correlated electronic states in La-Sr-Cu and Y-Ba-Cu oxides. *Phys. Rev. B* **35**, 8814-8817 (1987).
[28] Shen, Z.-X. *et al.* Electronic structure of Bi-Ca-Sr-Cu-O superconductors studied by photoelectron spectroscopy. *Phys. Rev. B* **38**, 7152-7155 (1988).
[29] Shen, Z.-X. and Dessau, D.S. Electronic structure and photoemission studies of late transition-metal oxides – Mott insulators and high-temperature superconductors. *Rhys. Rep.* **253**, 1-162 (1995).
[30] Lin, H. *et al.* Raising BiO bands above the Fermi energy level of hole-doped $Bi_2Sr_2CaCu_2O_{8+\delta}$ and other cuprate superconductors. *Phys. Rev. Lett.* **96**, 097001 (2006).
[31] McElroy, K. *et al.* Atmoic-scale sources and mechanism of nanoscale electronic disorder in $Bi_2Sr_2CaCu_2O_{8+\delta}$. *Science* **309**, 1048-1052 (2005).
[32] Giannozzi, P. *et al.* QUANTUM ESPRESSO: a modular and open-source software project for quantum simulations of materials. *J. Phys.:Condens. Matter* **21,** 395502 (2009).
[33] Perdew, J. P., Burke, K., Ernzerhof, M., Generalized Gradient Approximation Made Simple. *Phys. Rev. Lett.* **77** 3865-3868 (1996).
[34] Hamann, D. R. Optimized norm-conserving Vanderbilt pseudopotentials. *Phys. Rev. B* **88**, 085117 (2013).